Migration of an Excess Proton upon Asymmetric Hydration: $H^+[(CH_3)_2O](H_2O)_n$ as a Model System

Hai-Chou Chang,[†] Jyh-Chiang Jiang,[†] Ina Hahndorf,[†] Sheng H. Lin,[†,‡] Yuan T. Lee,[†,‡] and Huan-Cheng Chang*[,†]

Contribution from the Institute of Atomic and Molecular Sciences, Academia Sinica, P.O. Box 23-166, Taipei, Taiwan 106, R.O.C., and Department of Chemistry, National Taiwan University, Taipei, Taiwan 106, R.O.C.

Received September 21, 1998

Abstract: An excess proton can migrate from a solute to solvent molecules upon asymmetric solvation. The migration depends sensitively on solvation number, solvation structure, and proton affinity differences between solute and solvent molecules. The present study demonstrates this intriguing solvation-induced effect using protonated dimethyl ether−water clusters as the benchmark system. An integrated examination of $H^+[(CH_3)_2O](H_2O)_n$ by vibrational predissociation spectroscopy and ab initio calculations indicates that the excess proton is (1) localized on $(CH_3)_2O$ at $n = 1$, (2) equally shared by $(CH_3)_2O$ and $(H_2O)_2$ at $n = 2$, and (3) completely transferred to $(H_2O)_n$ at $n \geq 3$. The dynamics of proton transfer is revealed by the characteristic free- and hydrogen-bonded-OH stretching vibrations of the water molecules in direct contact with the excess proton. Both hydrogen bond cooperativity and zero-point vibrations have crucial influences on the final position of the proton in the clusters. Further insight into this remarkable phenomenon of intracluster proton transfer is provided by a comparison between $H^+[(CH_3)_2O](H_2O)_n$ and its structural analogues, $H^+(H_2O)_{n+1}$ and $H^+[(C_2H_5)_2O](H_2O)_n$.

Introduction

Proton transfer is a common and essential reaction in various chemical and biological systems.[1] It occurs swiftly because of the quantum nature of the proton.[2] In aqueous solutions, transfer of an excess proton is one of the key steps in acid- and enzyme-catalyzed reactions.[3] Water often heavily participates in these processes by accepting and/or donating protons.[4] A systematic study of proton migration in water clusters is important from the perspective that it can provide prerequisite knowledge for a thorough understanding of acid-, base-, and enzyme-catalyzed reactions at a microscopic level.[5] Theoretical analysis of water-mediated proton-transfer reactions, such as amide hydrolysis,[6] enzyme catalysis,[7] and the migration of an excess proton along an ion channel,[8] is emerging.

A fundamental question in solution chemistry concerns how an excess proton can migrate from a solute to solvent molecules upon solvation. Recent ab initio molecular dynamics calculations[9] have actively examined the exceptionally large mobility of a proton in liquid water. A mechanism of proton transfer mediated by periodic interconversion between $H_3O^+(H_2O)_n$ and $H_5O_2^+(H_2O)_{n-1}$ is simulated.[9,10] The theoretical endeavors, together with experimental findings, have established a fairly good understanding of the proton-transfer behaviors in protonated water clusters.[11] In solute-containing water clusters, however, the nature of this transfer is less obvious. The process is expected to depend sensitively on solvation number, solvent arrangement, and proton affinity differences between solute and solvent molecules.

The solvation-induced proton transfer is a general phenomenon that occurs in a wide range of organic bases. The phenomenon can be dramatic for molecules which display marked differences in their gas- and condensed-phase basicities. Trimethylamine, for example, has a gas-phase proton affinity (PA) of 225 kcal/mol,[12] which exceeds that of pyridine by 3 kcal/mol; hence, it is considered as a stronger base than pyridine in the gas phase. However, trimethylamine becomes a much weaker base in aqueous solutions with a pK_b of 9.80 versus 5.25 of pyridine.[13] The reversed order in basicity reflects the strong influence of solvation environment, which can be asymmetric, on the electronic structures of these molecules in liquid water.[14] Previous spectroscopic measurements have

* E-mail: hcchang@po.iams.sinica.edu.tw.
† Academia Sinica.
‡ National Taiwan University.

(1) See the special issue of *Ber. Bunsen-Ges. Phys. Chem.* **1998**, *102*, 2.
(2) Marcus, R. A. *Faraday Discuss. Chem. Soc.* **1982**, *74*, 7.
(3) Fersht, A. *Enzyme Structure and Mechanism*; New York: Freeman, 1985.
(4) Kandori, H.; Yamazaki, Y.; Sasaki, J.; Needleman, R.; Lanyi, J. K.; Maeda, A. *J. Am. Chem. Soc.* **1995**, *117*, 2118.
(5) Achatz, U.; Joos, S.; Berg, C.; Schindler, T.; Beyer, M.; Albert, G.; Niedner-Schatteburg, G.; Bondybey, V. E. *J. Am. Chem. Soc.* **1998**, *120*, 1876.
(6) Antonczak, S.; Ruiz-López, M. F.; Rivail, J. L. *J. Am. Chem. Soc.* **1994**, *116*, 3912.
(7) Lu, D.; Voth, G. A. *J. Am. Chem. Soc.* **1998**, *120*, 4006.
(8) Pomès, R.; Roux, B. *J. Phys. Chem.* **1996**, *100*, 2519. Drukker, K.; de Leeuw, S. W.; Hammes-Schiffer, S. *J. Chem. Phys.* **1998**, *108*, 6799.
(9) Tuckerman, M.; Laasonen, K.; Sprik, M.; Parrinello, M. *J. Phys. Chem.* **1995**, *99*, 5749. Tuckerman, M.; Laasonen, K.; Sprik, M.; Parrinello, M. *J. Chem. Phys.* **1995**, *103*, 150.
(10) Lobaugh, J.; Voth, G. A. *J. Chem. Phys.* **1996**, *104*, 2056. Pavese, M.; Voth, G. A. *Ber. Bunsen-Ges. Phys. Chem.* **1998**, *102*, 527.
(11) Agmon, N. *Chem. Phys. Lett.* **1995**, *244*, 456.
(12) Hunter, E. P. L.; Lias, S. G. *J. Phys. Chem. Ref. Data* **1998**, *27*, 413.
(13) Lide, D. R., Ed. *CRC Handbook of Chemistry and Physics*, 75th ed.; CRC Press: Boca Raton, FL, 1994.
(14) The effect of solvation structures on solute basicities has been theoretically scrutinized for methylamines in aqueous solutions. See, for example: Kawata, M.; Ten-no, S.; Kato, S.; Hirata, F. *Chem. Phys.* **1996**, *203*, 53.

10.1021/ja983353v CCC: $18.00
Published on Web 04/24/1999

explored the transfer of a proton in clusters with this solvation asymmetry in the gas phase.[15−18] These studies, however, were confined to electronically excited neutral clusters[15,16] or clusters containing photoionized species.[17,18] The present work extends the exploration to solvation-induced proton transfer in protonated solute-containing water clusters at ground electronic states. It is aimed to provide snapshots of proton transfer in the early phase of hydration.

There has been some earnest search of solvation-induced proton transfer for protonated organic bases. Employing ab initio calculations, Deakyne et al.[19] predicted this process to occur at $n = 2$ of $CH_3CNH^+-(H_2O)_n$, on the basis that CH_3CN has a PA (186.2 kcal/mol) higher than that of water by 21 kcal/mol.[12] El-Shall, Meot-Ner, and co-workers[20] examined water−methanol−trimethylamine clusters in a joint beam expansion/thermochemical experiment. They concluded that, while the PA of water is lower than that of methanol and trimethylamine, the excess proton can be preferentially taken by H_2O, owing to effective hydrogen bond blocking by methyl groups. Schindler et al.[21] investigated $H^+[(C_2H_5)_2O]_m(H_2O)_n$ in a Fourier transform ion cyclotron resonance cell and accordingly found exceptionally stable clusters appearing at the solvation numbers of $m = n + 2$ with protonated water ion cores. There remains, however, a lack of *spectroscopic* evidence to support the existence of H_3O^+-centered structures and solvation-induced proton transfers in these cluster systems.

Infrared spectroscopy, in conjunction with ab initio calculations, is becoming one of the most powerful tools in characterizing neutral and ionic clusters. By matching the observed spectra with the calculated stick diagrams, useful information concerning the structures and dynamics of the clusters of interest can be obtained. This approach has been successfully employed for studying neutral water polymers[22] and ionic water-containing clusters[23,24] generated in a molecular beam. One unique feature of the protonated cluster ions is that they possess excess protons. Locating the positive charge in a cluster is challenging and has been rarely attempted using infrared spectroscopy in the gas phase.[25] As will be demonstrated in this article, both free- and hydrogen-bonded-OH stretching frequencies of the water molecules in direct contact with the charge are sensitive to the location of the excess proton in protonated solute-containing water clusters. From systematic investigations of the changes in frequency of these two stretches as a function of proton location, elucidation of the proton-transfer behaviors within a cluster is possible.

Protonated dimethyl ether−water clusters serve as a model system for this study. The solvation of $(CH_3)_2OH^+$ by H_2O is highly asymmetric, thanks to the hydrophobic nature of the methyl groups on the solute molecule. In hydration energy measurements of $(CH_3)_2OH^+$, Kebarle and co-workers[26] observed a difference in basicity between $H^+(H_2O)_{n+1}$ and $H^+[(CH_3)_2O](H_2O)_n$, and the difference decreases smoothly with increasing n. They speculated from these observations that the basicity of H_2O might be higher than that of $(CH_3)_2O$ in aqueous solutions, a behavior opposite to their gas-phase PA ordering of 165 versus 189 kcal/mol for H_2O and $(CH_3)_2O$, respectively.[12] In this work, we seek to provide both spectroscopic and computational evidence for the occurrence of solvation-induced proton transfer in this cluster system. In addition to $H^+[(CH_3)_2O](H_2O)_n$, protonated diethyl ether water clusters were examined to delineate a more comprehensive picture.

Methodologies

A. Vibrational Predissociation Spectroscopy. The experiment was conducted using a vibrational predissociation ion trap spectrometer coupled with a pulsed infrared laser system as described previously.[24] We generated protonated dimethyl ether ions by corona-discharging a flow of $(CH_3)_2O/H_2O$ vapor seeded in pure H_2. The ions formed clusters with neutral water molecules through supersonic expansion. Such synthesized clusters, after size selection by a sector magnet mass filter, were injected into an octopole ion trap for spectroscopic measurements. Upon resonant excitation of OH stretches, the size-selected cluster ions dissociated predominantly via unimolecular loss of water molecules as

$$H^+[(CH_3)_2O](H_2O)_n \xrightarrow{h\nu} H^+[(CH_3)_2O](H_2O)_{n-1} + H_2O \quad (1)$$

Production of the photofragments was monitored by a second mass filter, from which infrared spectra were obtained by recording the concentration increase of $H^+[(CH_3)_2O](H_2O)_{n-1}$ as a function of laser wavelength.

Prior flow tube measurements[27] indicated that ion−molecule association can occur when $(CH_3)_2OH^+$ collides with H_2O at low energies. The excess proton remains firmly attached to the ether after collisions, as the proton affinity of water is lower than $(CH_3)_2O$ by 24 kcal/mol.[12] Conversion of $(CH_3)_2OH^+$ to $CH_3CH_2OH_2^+$ during corona discharge in this experiment is unlikely to occur since a high potential barrier exists between these two isomeric forms.[28] The structural isomerization between $(CH_3)_2OH^+$ and $CH_3CH_2OH_2^+$ is expected to have a minor contribution to the present observations.

B. Ab Initio Calculations. The ab initio calculations were carried out using the Gaussian 94 program package at the B3LYP/6-31+G* level. The calculations provided structures, binding energies, harmonic vibrational frequencies, and infrared absorption intensities of various structural isomers to be compared with measurements. A single scaling factor (0.973), chosen by referring to the free-OH stretching of 2- and 3-coordinated H_2O molecules,[23] was used for the calculated frequencies.[29] In this work, we closely examined the potential energy surface along the proton-transfer coordinate involving the $O-H^+\cdots O$ hydrogen bond in both $H^+[(CH_3)_2O](H_2O)_2$ and $H^+[(CH_3)_2O](H_2O)_3$ clusters. The nonadditive contribution of the energy due to hydrogen bond cooperativity (E_{HB}) was evaluated by

$$E_{HB} = E_T - E(E_m-H^+\cdots W) - E(W\cdots W) \quad (2)$$

(15) Bernstein, E. R. *Annu. Rev. Phys. Chem.* **1995**, *46*, 197 and references therein.
(16) Syage, J. A. *J. Phys. Chem.* **1995**, *99*, 5772 and references therein.
(17) Ebata, T.; Fujii, A.; Mikami, N. *Int. J. Mass Spec. Ion Processes* **1996**, *159*, 111. Sato, S.; Mikami, N. *J. Phys. Chem.* **1996**, *100*, 4765.
(18) Choi, J.-H.; Kuwata, K. T.; Haas, B.-M.; Cao, Y.; Johnson, M. S.; Okumura, M. *J. Chem. Phys.* **1994**, *100*, 7153.
(19) Deakyne, C. A.; Meot-Ner, M.; Campbell, C. L.; Hughes, M. G.; Murphy, S. P. *J. Chem. Phys.* **1986**, *84*, 4958.
(20) El-Shall, M. S.; Daly, G. M.; Gao, J. L.; Meot-Ner, M.; Sieck, L. W. *J. Phys. Chem.* **1992**, *96*, 507.
(21) Schindler, T.; Berg, C.; Niedner-Schatteburg, G.; Bondybey, V. E. *Chem. Phys. Lett.* **1995**, *201*, 491.
(22) Gruenloh, C. J.; Carney, J. R.; Arrington, C. A.; Zwier, T. S.; Fredericks, S. Y.; Jordan, K. D. *Science* **1997**, *276*, 1678. Buck, U.; Ettischer, I.; Melzer, M.; Buch, V.; Sadlej, J. *Phys. Rev. Lett.* **1998**, *80*, 2578.
(23) Wang, Y.-S.; Jiang, J. C.; Cheng, C.-L.; Lin, S. H.; Lee, Y. T.; Chang, H.-C. *J. Chem. Phys.* **1997**, *107*, 9695. Jiang, J. C.; Chang, J.-C.; Wang, B.-C.; Lin, S. H.; Lee, Y. T.; Chang, H.-C. *Chem. Phys. Lett.* **1998**, *289*, 373.
(24) Wang, Y.-S.; Chang, H.-C.; Jiang, J. C.; Lin, S. H.; Lee, Y. T.; Chang, H.-C. *J. Am. Chem. Soc.* **1998**, *120*, 8777.
(25) Chang, H.-C.; Jiang, J. C.; Lin, S. H.; Lee, Y. T.; Chang, H.-C. *J. Phys. Chem.* In press. Chang, H.-C.; Jiang, J. C.; Chang, H.-C.; Wang, L. R.; Lee, Y. T. *Israel J. Chem.* In press.
(26) Hiraoka, K.; Grimsrud, E. P.; Kebarle, P. *J. Am. Chem. Soc.* **1974**, *96*, 3359.
(27) Matthews, K. K.; Adams, N. G. *Int. J. Mass Spectrom. Ion Processes* **1997**, *163*, 221.
(28) Fairley, D. A.; Scott, G. B. I.; Freeman, C. G.; Maclagan, G. A. R.; McEwan, M. J. *J. Phys. Chem. A* **1997**, *101*, 2848.
(29) Jiang, J. C.; Chang, H.-C.; Lee, Y. T.; Lin, S. H. *J. Phys. Chem.* In press.

Table 1. Ab Initio Calculated Proton Affinities and Gas Basicities (kcal/mol) Using B3LYP/6-31+G* and Their Comparisons with Experimental Values at 298 K

	calcd			expt[b]	
species	ΔE^a	ΔH^{298}	ΔG^{298}	$\Delta H°(298)$	$\Delta G°(298)$
H_2O	−160.5	−162.0	−154.7	−165.2	−157.7
$(H_2O)_2$	−192.1	−194.2	−185.0	−193.2[d]	−184.0[d]
$(H_2O)_3$	−211.4[c]	−213.7[c]	−203.7[c]	−211[d]	−199[d]
$(CH_3)_2O$	−184.5	−185.8	−178.6	−189.3	−182.7
$(C_2H_5)_2O$	−194.0	−195.2	−188.0	−198.0	−191.4

[a] Energy of protonation. [b] Reference 12. [c] Proton affinity of the water molecule situated in the middle of $H_2O\cdots HOH\cdots OH_2$. [d] Estimated from the dissociation energies of $H_5O_2^+$ (ref 31) and $(H_2O)_2$ (ref 30).

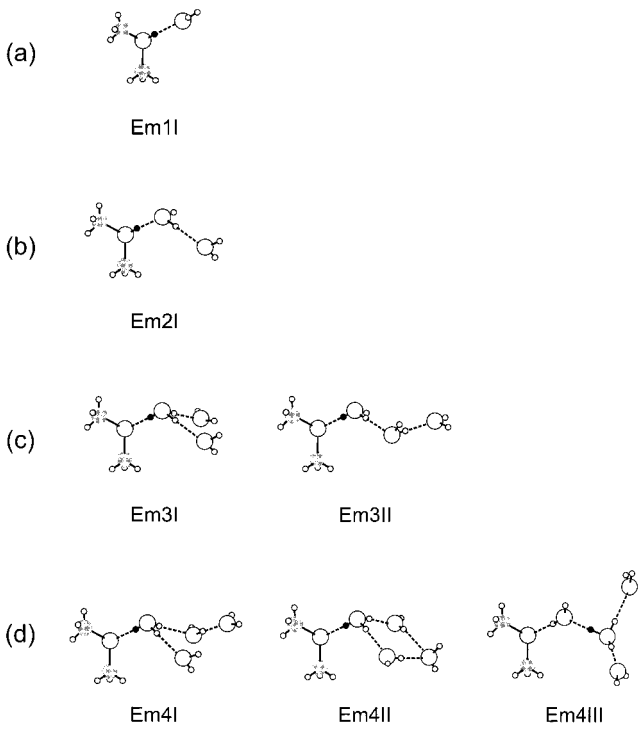

Figure 1. Ab initio optimized structures of $H^+[(CH_3)_2O](H_2O)_{1-4}$ clusters. The C, O, and H atoms are denoted by a shaded circle, large open circle, and small open circle, respectively, but with the transferring proton denoted by a small solid circle.

where E_T is the total interaction energy and $E(E_m-H^+\cdots W)$ and $E(W\cdots W)$ are the respective interaction energies of the dimers, with E_m denoting $(CH_3)_2O$ and W denoting H_2O.

As a test on the validity of the B3LYP/6-31+G* calculations, we first evaluated the proton affinity (PA) and gas basicity (GB) of the species involved in this experiment. Table 1 lists the calculated PA and GB to be compared with the measurements. For the water dimer, its proton affinity was estimated from the PA of water and the energetics of the clustering[30,31]

$$H_3O^+ + H_2O \rightarrow H^+(H_2O)_2 \qquad \Delta H° = -31.5 \text{ kcal/mol} \quad (3)$$

$$H_2O + H_2O \rightarrow (H_2O)_2 \qquad \Delta H° = -3.59 \text{ kcal/mol} \quad (4)$$

to obtain PA = 165.3 + 31.5 − 3.59 = 193.2 kcal/mol as the experimental value. Notably, in Table 1, all the calculated values of the monomers are systematically underestimated by 3−4 kcal/mol, whereas the predicted PA and GB of $(H_2O)_2$ fortuitously agree with the measurement within 1 kcal/mol. Figure 1 depicts the optimized geometries of the low-energy isomers of $H^+[(CH_3)_2O](H_2O)_{1-4}$ produced by the present B3LYP/6-31+G* calculations. Interestingly, both isomers **Em1I** and **Em2I** contain a $(CH_3)_2OH^+$ ion core, whereas the clusters of $n = 3$ and 4 are all H_3O^+-centered.

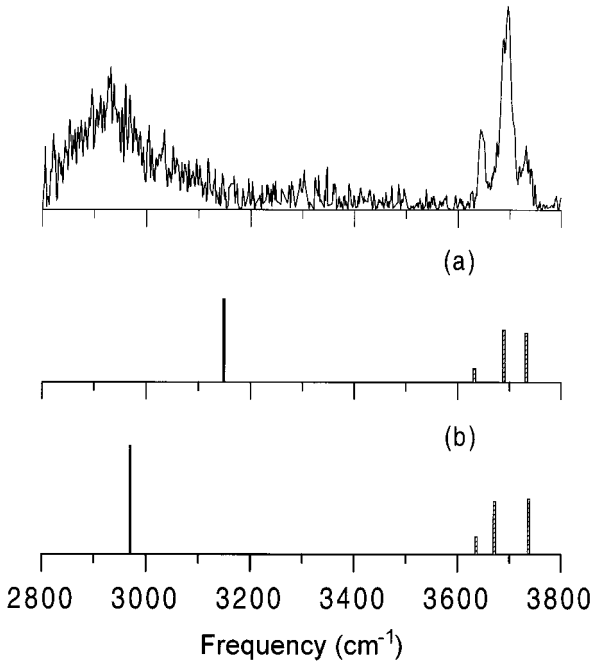

Figure 2. Vibrational predissociation spectrum of $H^+[(CH_3)_2O](H_2O)_2$ and its comparison with ab initio calculated stick diagrams of isomer **Em2I**. The calculated CH stretching features, situated at ∼3000 cm^{-1}, have absorption intensities about 10-fold lower than that of OH. The two stick diagrams are obtained based on the lowest-energy geometries (a) before and (b) after taking into account zero-point vibrational effects (Figure 5). Note that the intensities of free-OH stretches (▨) have been multiplied by a factor of 5 for clearer comparison with that of the bonded-OH stretches (■).

Results and Analysis

Four distinct OH stretching features were observed for $H^+[(CH_3)_2O](H_2O)_2$ in the frequency range of 2700−3900 cm^{-1} (cf. Figure 2).[32] A comparison between the experimentally observed spectrum and the ab initio calculated stick diagram of isomer **Em2I** allows for an assignment of these absorption bands in Table 2. There are two types of water molecules in this cluster: one acts as a single proton acceptor (A) in the second (2°) solvation shell and the other acts concurrently as a single proton acceptor and a single donor (AD) in the first (1°) solvation shell of the $(CH_3)_2OH^+$ ion core. They gives rise to three free-OH stretches at 3645, 3693, and 3732 cm^{-1} and one hydrogen-bonded-OH stretch at 2939 cm^{-1}. Note that in Figure 2a and Table 2, the predicted bonded-OH stretching frequency is significantly overestimated by ∼200 cm^{-1} in the case of using 0.973 as the scaling factor for the B3LYP/6-31+G* calculations.

Figure 3 compares the OH stretching spectrum of $H^+[(CH_3)_2O](H_2O)_3$ and the calculated stick diagrams of two low-energy isomers, **Em3I** and **Em3II** (Figure 1c). Apparently, **Em3I**, which is lower in energy than **Em3II** (cf. Table 3), holds an excellent fit to the observed spectrum. This lowest-energy isomer, with C_s symmetry, has an H_3O^+ ion core and two essentially identical single-acceptor H_2O molecules which display two identical (within the present spectral resolution) sets of symmetric and asymmetric free-OH stretches. This explains

(30) Curtiss, L. A.; Frurip, D. L.; Blander, M. *J. Chem. Phys.* **1979**, *71*, 2703.

(31) Meot-Ner, M. *J. Am. Chem. Soc.* **1984**, *106*, 1265.

(32) An attempt to obtain the vibrational predissociation spectrum of the cluster of $n = 1$ was unsuccessful because the hydrogen bonding ($\Delta H°_D$ = 22.6 kcal/mol) between $(CH_3)_2OH^+$ and H_2O is too strong for the single-photon dissociation to occur.

Table 2. Observed and Calculated Frequencies (cm^{-1}) of the Free- and Bonded-OH Stretches of $H^+[(CH_3)_2O](H_2O)_n$, $n = 1-4$

species	frequency obsd	frequency calcd[a]	isomers[b]	assignments[c]
$H^+[(CH_3)_2O](H_2O)$		3725	**Em1I**	asymmetric free-OH of 1°H_2O(A)
		3627	**Em1I**	symmetric free-OH of 1°H_2O(A)
		2626	**Em1I**	bonded-OH of $(CH_3)_2OH^+$
$H^+[(CH_3)_2O](H_2O)_2$	3732	3733	**Em2I**	asymmetric free-OH of 2°H_2O(A)
	3693	3689	**Em2I**	free-OH of 1°H_2O(AD)−A
	3645	3632	**Em2I**	symmetric free-OH of 2°H_2O(A)
	2939	3149	**Em2I**	bonded-OH of 1°H_2O(AD)−A
		1836	**Em2I**	bonded-OH of $(CH_3)_2OH^+$
$H^+[(CH_3)_2O](H_2O)_3$	3732	3734, 3732	**Em3I**	asymmetric free-OH of 1°H_2O(A)
	3645	3633, 3632	**Em3I**	symmetric free-OH of 1°H_2O(A)
	3200		**Em3II**[d]	bonded-OH of 1°H_2O(AD)−A
	2974	2994	**Em3I**	asymmetric bonded-OH of H_3O^+−A
	2914	2941	**Em3I**	symmetric bonded-OH of H_3O^+−A
		2175	**Em3I**	bonded-OH of H_3O^+−E
$H^+[(CH_3)_2O](H_2O)_4$	3738	3748	**Em4I**	asymmetric free-OH of 2°H_2O(A)
	3738	3735	**Em4I**	asymmetric free-OH of 1°H_2O(A)
	3711	3705	**Em4I**	free-OH of 1°H_2O(AD)−A
	3650	3643	**Em4I**	symmetric free-OH of 2°H_2O(A)
	3650	3633	**Em4I**	symmetric free-OH of 1°H_2O(A)
	3510		**Em4II**[d]	bonded-OH of 1°H_2O(AD)−AA
	3316	3310	**Em4I**	bonded-OH of 1°H_2O(AD)−A
	2995	3034	**Em4I**	bonded-OH of H_3O^+−A
		2581	**Em4I**	bonded-OH of H_3O^+−E
		2428	**Em4I**	bonded-OH of H_3O^+−AD

[a] Frequencies of the lowest-energy isomers of $n = 1-4$. [b] Structures illustrated in Figure 1. [c] The abbreviations used to describe the form of hydrogen bonding for H_2O are as follows: single-acceptor (A), double-acceptor (AA), and single-acceptor-single-donor (AD) in the first (1°) or second (2°) solvation shell of either the $(CH_3)_2OH^+$ or H_3O^+ ion core (cf. Figure 1). The dashes denote hydrogen bonding to the perturbing ether (E) or H_2O in the form of A or AA (see text for details). [d] Tentative assignments.

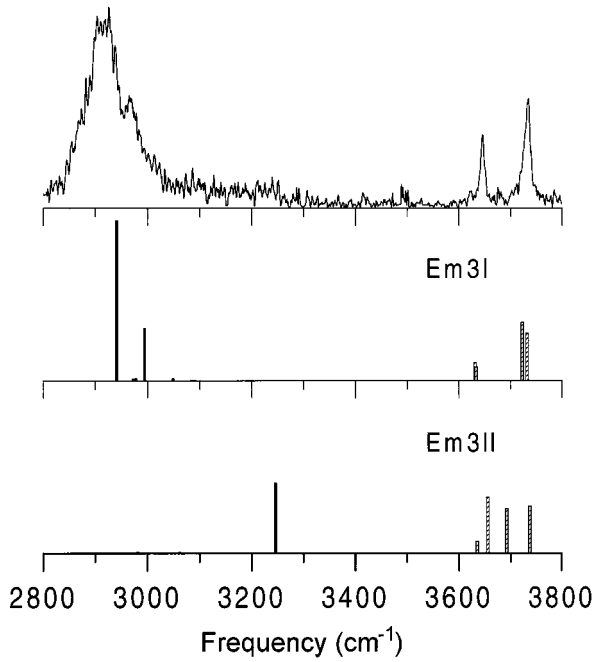

Figure 3. Vibrational predissociation spectrum of $H^+[(CH_3)_2O](H_2O)_3$ and its comparison with the ab initio calculated stick diagrams of isomers **Em3I** and **Em3II**. The calculated CH stretching features, situated at ~3000 cm^{-1}, have absorption intensities about 10-fold lower than that of OH. Note that the intensities of free-OH stretches (▨) have been multiplied by a factor of 5 for clearer comparison with that of the bonded-OH stretches (■).

why only two well-separated free-OH stretches at 3645 and 3732 cm^{-1} were observed for $H^+[(CH_3)_2O](H_2O)_3$. In the same spectrum, indications for the presence of isomer **Em3II** were also found: the characteristic bonded-OH stretching absorption of the 1°H_2O(AD) molecule is observed as a broad feature at ~3200 cm^{-1}. However, the absence of the free-OH stretching absorptions of the H_3O^+ ion core and the 1°H_2O molecule at ~3700 cm^{-1} (see the stick diagram of **Em3II** in Figure 3) prevents a conclusive identification of this isomer.

Ab initio calculations predicted three low-energy isomers for clusters with $n = 4$, **Em4I**, **Em4II**, and **Em4III** (Figure 1d), and their computed stick diagrams are stacked up against the observed spectrum of $H^+[(CH_3)_2O](H_2O)_4$ in Figure 4. The comparison unambiguously confirms the existence of **Em4I** in the supersonic expansion based upon the characteristic bonded-OH stretches at 2995 and 3316 cm^{-1}. To identify other isomers, a systematic temperature dependence measurement[24] was made from 160 to 200 K, but only minor changes were observed in the spectra. The invariance of the spectrum with temperature changes leads to the conclusion that **Em4I** is the lowest-energy isomer of $H^+[(CH_3)_2O](H_2O)_4$, in accord with the computational finding that **Em4I** is more strongly bound than **Em4II** and **Em4III** by ~1 kcal/mol in ΔE_n (cf. Table 3). It is likely that the weak feature at 3510 cm^{-1} in Figure 4 is derived from the ring-shaped isomer **Em4II**; unfortunately, this feature is too weak for an explicit assignment. Figure 1d also depicts the structure of isomer **Em4III**, in which the ether molecule is situated on the second solvation shell of the hydronium ion core. This structure is higher in energy than **Em4I** by ~1.5 kcal/mol, and it is not clearly identified by the present experiment.

It is instructive to compare the calculated absorption strengths with the experimentally observed intensities. Direct comparison of these numbers, however, should be made with caution since the intensities of the bands observed in vibrational predissociation spectra are a convoluted product of abundance, absorption, and dissociation cross sections; it may not be appropriate to use them to deduce the relative oscillator strengths of the OH stretches directly. Furthermore, in a prior experiment,[24] we determined that the vibrationally induced photodissociation discussed herein is a one-photon process. The dissociation is made possible at an expense of internal energies (~2 kcal/mol) contained in these clusters. Hence, the effective photodissocia-

Table 3. Ab Initio Calculated Total Energies (kcal/mol) of the Clustering Reactions $(CH_3)_2OH^+ + nH_2O \rightarrow H^+[(CH_3)_2O](H_2O)_n$ (I) and $(CH_3)_2O + H_3O^+ + (n-1)H_2O \rightarrow H^+[(CH_3)_2O](H_2O)_n$ (II), and Their Comparison with the Experimental Values at 298 K

	calcd[a]			expt (I)[b]		expt (II)[c]	
isomers[d]	ΔE_n	ΔH_n^{298}	ΔG_n^{298}	$\Delta H°_n(298)$	$\Delta G°_n(298)$	$\Delta H°_n(298)$	$\Delta G°_n(298)$
Em1I	−22.9	−23.2	−15.5	−22.6	−14.6		
Em2I	−37.1	−38.3	−21.4	−37.9	−22.1		
Em3I	−75.7	−76.9	−54.1			−75.8	−53.3
Em3II	−73.2	−74.7	−51.5				
Em4I	−86.5	−88.1	−55.3			−86.0	−57.8
Em4II	−85.8	−88.3	−52.8				
Em4III	−85.3	−86.6	−53.7				

[a] With both basis set superposition errors and zero-point vibrational energies corrected. [b] Reference 26. [c] Calculated from ref 26 using the proton affinity difference of PA[$(CH_3)_2O$] − PA(H_2O) = 24.1 kcal/mol and the gas basicity difference of GB[$(CH_3)_2O$] − GB(H_2O) = 25.0 kcal/mol (ref 12). [d] Structures illustrated in Figure 1.

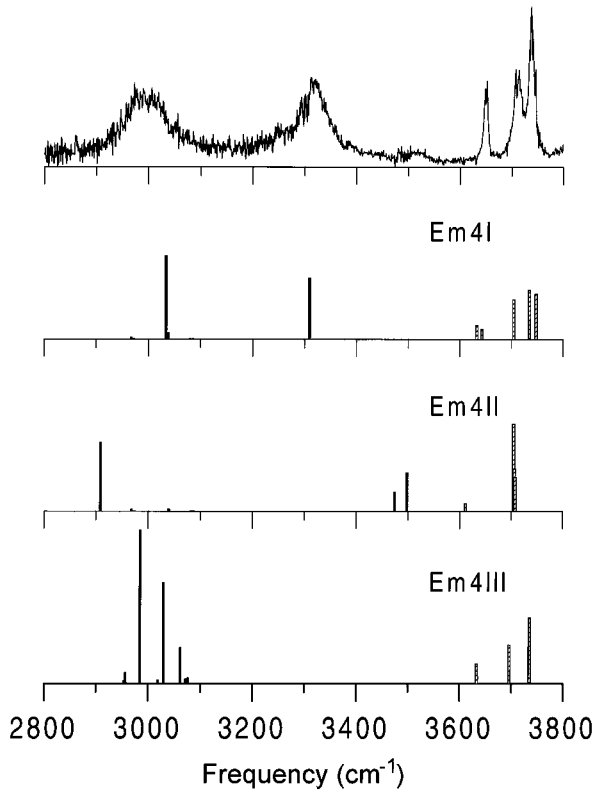

Figure 4. Vibrational predissociation spectrum of $H^+[(CH_3)_2O](H_2O)_4$ and its comparison with the ab initio calculated stick diagrams of isomers **Em4I**, **Em4II**, and **Em4III**. The calculated CH stretching features, situated at ~3000 cm^{-1}, have absorption intensities about 10-fold lower than that of OH. Note that the intensities of free-OH stretches (⍁) have been multiplied by a factor of 5 for clearer comparison with that of the bonded-OH stretches (■).

tion cross sections can be a sensitive function of input photon energies. Since the typical frequency difference between free- and hydrogen-bonded-OH stretches in Table 2 is more than 350 cm^{-1}, which amounts to half of the internal energy, the former can have a considerably larger cross section than the latter. As a result, the free-OH stretching absorptions can appear more pronounced in the observations, contradictory to the calculations.

Another noticeable feature of the spectra is that the bonded-OH absorption bands at ~3000 and ~3300 cm^{-1} of $n = 3$ and 4 are both narrower than that at ~2900 cm^{-1} of $n = 2$. The latter has a typical full width at half-maximum (fwhm) of 200 cm^{-1}, compared to the fwhm ≤ 100 cm^{-1} of the former at a cluster temperature of 180 K. This substantially larger width at $n = 2$ reflects the effect of proton delocalization which, conceivably, can broaden the associated absorption band profile. The CH stretches resonant in the same frequency region should not be responsible for this broadening since they are all much lower in oscillator strength than OH stretches in these three clusters (see the stick spectra in Figures 2−4).

Discussion

In a recent study,[25] we investigated the transfer dynamics of an excess proton in protonated methanol clusters employing the same techniques. It is demonstrated therein that the H^+ in $H^+(CH_3OH)_n$ can be either localized on one methanol unit or delocalized between two methanol molecules, depending on the structures of the clusters. A similar phenomenon was found in protonated water clusters.[33] The proton delocalization, or partial proton transfer, is an expected property of homogeneous dimers which contain two identical subunits. In heterogeneous clusters, proton delocalization can also occur, provided that two constituent subunits are comparable in proton affinity. To understand the proton-transfer behavior in heterogeneous clusters, useful information can be obtained from the solvation energy of the protonated ions of interest. In homogeneous dimers such as $H^+(H_2O)_2$ and $H^+(CH_3OH)_2$, the linking hydrogen bond is unusually strong owing to significant covalent bonding[34] between two identical units. Meot-Ner[35] has given a report on the dissociation energy ($\Delta H°_D$) of protonated dimers and empirically found that $\Delta H°_D$ is inversely proportional to the PA difference (ΔPA) between two constituents, with a linear correlation of $\Delta H°_D$ (kcal/mol) = 30.4 − 0.30ΔPA for $-OH^+\cdots O-$ bonds. An application of this correlation to $(CH_3)_2O-H^+-(H_2O)_2$, with ΔPA = 3.2 kcal/mol (Table 1), estimates a binding energy of $\Delta H°_D$ = 29.5 kcal/mol between $(CH_3)_2OH^+$ and $(H_2O)_2$. This agrees satisfactorily with the energetics

$$(CH_3)_2OH^+ + (H_2O)_2 \rightarrow H^+[(CH_3)_2O](H_2O)_2 \qquad \Delta H° = -34 \text{ kcal/mol} \quad (5)$$

obtained from eq 4 and the following addition reactions[26]

$$(CH_3)_2OH^+ + H_2O \rightarrow H^+[(CH_3)_2O](H_2O) \qquad \Delta H° = -22.6 \text{ kcal/mol} \quad (6)$$

$$H^+[(CH_3)_2O](H_2O) + H_2O \rightarrow H^+[(CH_3)_2O](H_2O)_2 \qquad \Delta H° = -15.3 \text{ kcal/mol} \quad (7)$$

Notably, the energy of $\Delta H° = -34$ kcal/mol is close to −31.5

(33) Jiang, J. C.; Wang, Y.-S.; Chang, H.-C.; Lin, S. H.; Lee, Y. T.; Niedner-Schatteburg, G.; Chang, H.-C. *J. Am. Chem. Soc.* Submitted for publication.
(34) Desmeules, P. J.; Allen, L. C. *J. Chem. Phys.* **1980**, *72*, 4731.
(35) Meot-Ner, M. *J. Am. Chem. Soc.* **1984**, *106*, 1257.

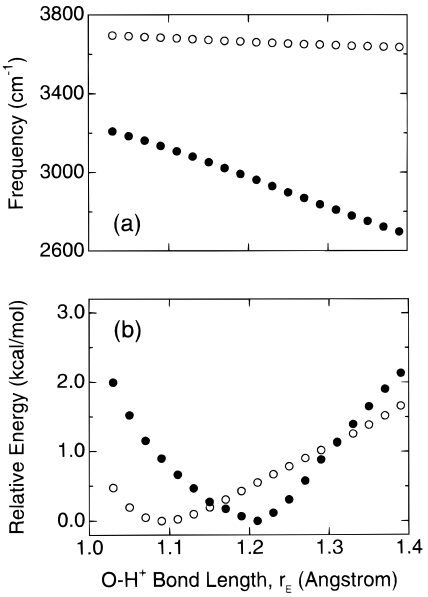

Figure 5. (a) Variation of the B3LYP-calculated free- (○) and hydrogen-bonded- (●) OH stretching frequencies with the position of the transferring proton in **Em2I**. (b) Variation of the B3LYP-calculated potential energies of **Em2I** with the O−H$^+$ bond length (r_E) of $(CH_3)_2O-H^+$ with (●) and without (○) ZPVE corrections. The changes of unconstrained interoxygen distances with r_E are shown in Figure 6.

kcal/mol of $H^+(H_2O)_2$ and −33 kcal/mol of $H^+(CH_3OH)_2$.[31] Proton delocalization is, hence, expected to occur in a manner similar to that of $H^+(H_2O)_2$ and $H^+(CH_3OH)_2$ in this heterogeneous cluster.

A. Size Dependence of Intracluster Proton Transfer. Figures 2−4 compare the theoretically calculated and experimentally observed bonded-OH stretching frequencies of $H^+[(CH_3)_2O](H_2O)_{2-4}$. A good agreement was reached for both $n = 3$ and 4, whereas a significant deviation occurred at $n = 2$. The deviation arises from the procedure that the spectrum displayed in Figure 2a was computed based on the optimized structure of $(CH_3)_2O-H^+\cdots(H_2O)_2$, in which the excess proton is firmly attached to the ether (Figure 1b). Together with the earlier bandwidth and energetics considerations, this deviation readily suggests a charge delocalization of the excess proton between $(CH_3)_2O$ and $(H_2O)_2$. An analysis of zero-point vibrational effects on proton location and OH stretching frequencies of the 1°H_2O molecule was, thus, performed to quantitatively assess this speculation. Figure 5b presents the ab initio calculated potential energy surface of $H^+[(CH_3)_2O](H_2O)_2$ along the r_E coordinate for isomer **Em2I**, where r_E is the O−H$^+$ bond length of the protonated ether. The corresponding changes of the interoxygen distance between $(CH_3)_2O$ and 1°H_2O are displayed in Figure 6. The excess proton is initially localized on dimethyl ether with an equilibrium bond length of $r_E = 1.092$ Å and $R_{OO} = 2.452$ Å. However, after taking zero-point vibrational energies (ZPVE) into account, a new minimum emerges at $r_E = 1.222$ Å and $R_{OO} = 2.423$ Å. This shift of energy minimum is a pure quantum effect, which plays a crucial role in clusters having fairly flat potential surfaces along the proton-transfer coordinate.[36]

The O−H$^+$ bond lengthening of 0.13 Å (1.092 → 1.222 Å), accompanied by an O−O distance shortening of 0.03 Å (2.452 → 2.423 Å), can dramatically alter the vibrational frequencies of the water molecule in direct contact with the proton. Figure 5a illustrates the dependence of both free- and hydrogen-bonded-OH stretching frequencies of the 1°H_2O(AD) molecule on r_E in isomer **Em2I**. The bonded-OH stretching frequency is highly sensitive to the proton position; it varies from 3200 to 2700 cm^{-1} as r_E increases from 1.05 to 1.40 Å. The free-OH stretch red-shifts only ∼50 cm^{-1} in comparison. As for the 2°H_2O(A) molecule, the variation of its free-OH stretching frequencies with r_E is even smaller, being ∼10 cm^{-1}/Å. By imposing this correction into the calculations, the match between the experimentally observed spectrum and the theoretically calculated stick diagram is greatly improved, as demonstrated in Figure 2b. The good agreement suggests a vibrationally averaged bond length of $\langle r_E \rangle \sim 1.2$ Å for $H^+[(CH_3)_2O](H_2O)_2$. This length is nearly half of the interoxygen distance of 2.42 Å, implying that the excess proton is equally shared by $(CH_3)_2O$ and $(H_2O)_2$ in this heterogeneous water cluster.

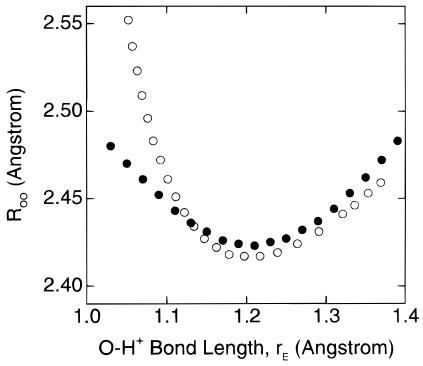

Figure 6. Variation of the B3LYP-calculated interoxygen distances between $(CH_3)_2O$ and 1°H_2O with the O−H$^+$ bond length (r_E) in isomers **Em2I** (●) and **Em3II** (○).

To understand the intracluster proton-transfer behavior, the competition for the excess proton between the solute and the solvent polymers was considered. Dimethyl ether has a PA of 189 kcal/mol, higher than that of water by 24 kcal/mol.[12] Hence, the proton should be localized on the ether in the binary complex $(CH_3)_2OH^+-H_2O$ (Figure 1a). For $H^+[(CH_3)_2O](H_2O)_2$, one would expect the proton to be taken by $(H_2O)_2$ since the PA (193.2 kcal/mol) of the water dimer is higher than that of $(CH_3)_2O$ by 4 kcal/mol. This PA difference, however, is somewhat marginal and it can be easily compensated for by hydrogen bond cooperative effects[37] which favor a localization of the excess proton on the ether side. As is well documented for cyclic water clusters,[38,39] the hydrogen bond cooperativity has a contribution up to 20% in total binding energy. This effect can be further enhanced in $(CH_3)_2O$ from the electron donation nature of the two alkyl groups.[39] The present calculations predict a hydrogen bonding nonadditivity of $E_{HB} = 11$ kcal/mol (eq 2), which forces the proton to locate at a site near the ether with $r_E = 1.092$ Å at the potential minimum. The hydrogen bond cooperativity, strikingly, governs the position of the excess proton in this cluster.

The hydrogen bond cooperativity plays a further prominent role in **Em3II**, where the water molecules are arranged in a linear array as $OH_2\cdots OH_2\cdots OH_2$. In this water trimer, the PA of the first water molecule is unknown, but is estimated to be

(36) A scan of the potential energy surface along r_E using MP2/6-31+G* also showed similar features for **Em2I**. The excess proton is initially localized at the potential minimum of $r_E = 1.07$ Å, but moves to $\langle r_E \rangle = 1.19$ Å upon averaging by zero-point vibrations.

(37) Cruzan, J. D.; Braly, L. B.; Liu, K.; Brown, M. G.; Loeser, J. G.; Saykally, R. J. *Science* **1996**, *271*, 59.
(38) Xantheas, S. S. *J. Chem. Phys.* **1995**, *102*, 4505.
(39) Masella, M.; Flament, J. P. *J. Chem. Phys.* **1998**, *108*, 7141 and references therein.

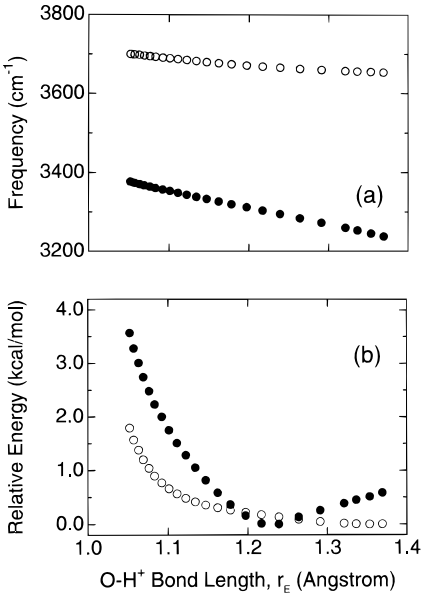

Figure 7. (a) Variation of the B3LYP-calculated free (○) and hydrogen-bonded (●) OH stretching frequencies with the position of the transferring proton in **Em3II**. (b) Variation of the B3LYP-calculated potential energies of **Em3II** with the O−H$^+$ bond length (r_E) of $(CH_3)_2O$−H$^+$ with (●) and without (○) ZPVE corrections. The changes of unconstrained interoxygen distances with r_E are shown in Figure 6.

∼200 kcal/mol. There is an expected increase of ∼10 kcal/mol in PA for this H_2O (from the dimer to the trimer), because of the attachment of the third water molecule. While this PA is considerably larger than that of $(CH_3)_2O$, the enhanced hydrogen bond cooperativity, owing to an additional hydrogen bond formation, can substantially reduce the depth of the potential well along the r_E coordinate. Figure 7b illustrates a scan of the potential energy surface along r_E in **Em3II**. The potential is rather flat over the range of $r_E = 1.1-1.4$ Å, allowing the zero-point vibrational effects to yield a new potential minimum at $r_E \sim 1.2$ Å. It is noteworthy that the zero-point vibrations have a less influential impact on **Em3II** than on **Em2I**, where an energy change of ∼1.5 kcal/mol is produced at $r_E = 1.093$ Å (Figure 5b). The excess proton in **Em3II**, consequently, can be found at a site closer to $(H_2O)_3$, with a vibrationally averaged bond length of O−H$^+$ longer than 1.21 Å.

Neither hydrogen bond cooperativity nor zero-point vibrational effects dominate the situation in isomer **Em3I**. For the middle water molecule in this trimer array, $H_2O\cdots HOH\cdots OH_2$, the proton affinity is estimated to be PA ∼ 165.3 + 31.5 + 20 − 6 = 211 kcal/mol, obtained from the hydration enthalpy[31]

$$H^+(H_2O)_2 + H_2O \rightarrow H^+(H_2O)_3 \qquad \Delta H^\circ = -20 \text{ kcal/mol} \tag{8}$$

and the dissociation energy of ∼3 kcal/mol per neutral hydrogen bond. The strength of ∼3 kcal/mol was assumed on the basis that the middle water molecule behaves like a double proton donor and, hence, each hydrogen bonding should be weaker than the one holding the dimer together (eq 4). Note that the PA of such a hydrogen-bonded water molecule is 211 kcal/mol, differing from that of $(CH_3)_2O$ by 22 kcal/mol. This PA difference is obviously too large to be compensated for by the hydrogen bond cooperative effect, and the excess proton can only be taken by water to produce a hydronium-centered structure (**Em3I** in Figure 1c). Since the potential well of this isomer is considerably deepened, the shift of the energy minimum along r_E due to zero-point vibrations is negligible.

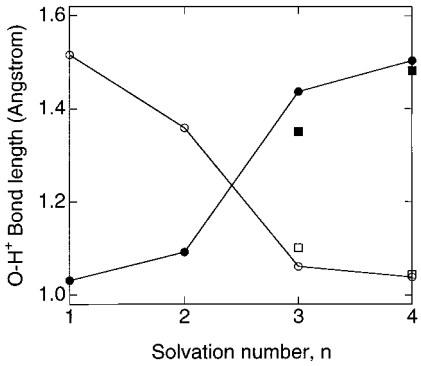

Figure 8. Ab initio calculated equilibrium bond length, r_E (● and ■) and r_W (○ and □), as a function of cluster sizes and geometries of $H^+[(CH_3)_2O](H_2O)_{1-4}$. The two isomers indicated in the plot are **Em3I** (circles) and **Em3II** (squares) at $n = 3$ and **Em4I** (circles) and **Em4II** (squares) at $n = 4$.

Last, the zero-point vibrations also have the effect of pulling the excess proton toward the ether in isomer **Em4I**. This effect, however, cannot match the driving force derived from the large PA difference (∼30 kcal/mol) between these two subunits. Therefore, the calculated frequencies can agree well with the observation in Figure 4 for isomer **Em4I**. Additional noteworthy features in Figure 4 are the frequencies of the two absorption bands observed at 2995 and 3316 cm^{-1}. They belong to the bonded-OH stretches of H_3O^+ and the 1°H_2O molecule perturbed by 1°H_2O and 2°H_2O, respectively. The large difference in frequency between these two stretches is directly correlated with their relative distances to the transferring proton. This direct correlation further demonstrates that infrared spectroscopy of OH stretches is a sensitive probe for proton-transfer reactions in protonated solute-containing water clusters.

The agreements between calculations and observations in Figures 2−4 allow for conclusive structural identification of the clusters of $n = 2-4$ (Table 2). Figure 8 presents an overview of the proton migration behavior, in terms of the calculated equilibrium bond length r_E, as a function of solvation number for $H^+[(CH_3)_2O](H_2O)_n$. The proton is seen to move from the ether side with $r_E = 1.031$ Å at $n = 1$ and $r_E = 1.092$ Å at $n = 2$, and toward the water side with $r_E = 1.437$ (1.351) Å at $n = 3$ and $r_E = 1.504$ (1.482) Å at $n = 4$ for isomers **Em1I**, **Em2I**, **Em3I** (**Em3II**), and **Em4I** (**Em4II**), respectively. The corresponding H$^+$−O bond lengths of the H_2O molecules in direct contact with the excess protons are $r_W = 1.516$, 1.359, 1.061 (1.101), and 1.038 (1.044) Å.

B. Comparison with Other Systems. To further understand how the PA of a solute molecule can change the vibrational frequencies of the bonded-OH stretches of 1°H_2O, we compared the spectra of $H^+[(CH_3)_2O](H_2O)_2$ and $H^+[(C_2H_5)_2O](H_2O)_2$ in Figure 9a. Two features deserve detailed examination. First, all the free-OH stretching frequencies of 1°H_2O and 2°H_2O agree within 1 cm^{-1} between these clusters. Second, the hydrogen-bonded-OH stretching frequency of the 1°H_2O in $H^+[(CH_3)_2O](H_2O)_2$ is lower than that in $H^+[(C_2H_5)_2O](H_2O)_2$ by 170 cm^{-1}. This large frequency difference in bonded-OH stretches clearly indicates that the positive charge is situated closer to water in $H^+[(CH_3)_2O](H_2O)_2$ than in $H^+[(C_2H_5)_2O](H_2O)_2$. This finding is in accord with the established measurement that the PA of diethyl ether exceeds that of dimethyl ether by 9 kcal/mol.[12]

Comparison can also be made among the spectra of $H^+(H_2O)_5$, $H^+[(CH_3)_2O](H_2O)_4$, and $H^+[(C_2H_5)_2O](H_2O)_4$. Ab initio calculations indicate that the lowest-energy isomers of

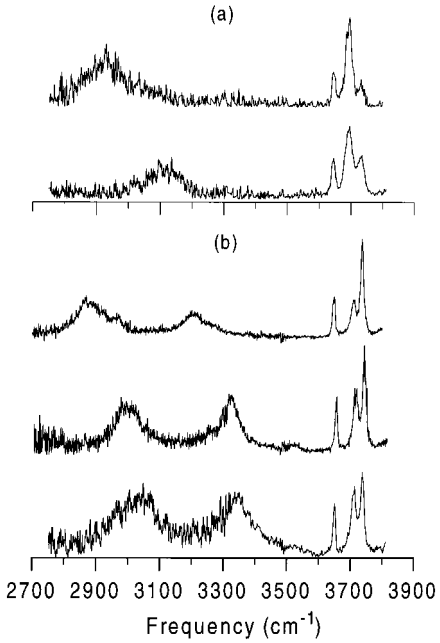

Figure 9. Comparison of the vibrational predissociation spectra between (a) $H^+[(CH_3)_2O](H_2O)_2$ and $H^+[(C_2H_5)_2O](H_2O)_2$ (top to bottom) and among (b) $H^+(H_2O)_5$, $H^+[(CH_3)_2O](H_2O)_4$, and $H^+[(C_2H_5)_2O](H_2O)_4$ (top to bottom).

both $H^+(H_2O)_5$ and $H^+[(C_2H_5)_2O](H_2O)_4$ are structurally similar to that of **Em4I** as

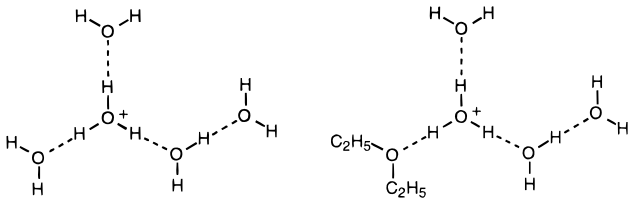

Figure 9b exhibits the spectrum of $H^+(H_2O)_5$ with free-OH stretches resonant at 3647, 3709, and 3736 cm^{-1} and bonded-OH stretches at 2879, 2967, and 3208 cm^{-1}.[33] These bonded-OH absorption bands are all substantially red-shifted from the corresponding features at 2995 and 3316 cm^{-1} of **Em4I**. An opposite trend, however, is observed for $H^+[(C_2H_5)_2O](H_2O)_4$, where the bonded-OH stretches at 3028 and 3340 cm^{-1} are all correspondingly blue-shifted by $\sim$30 cm^{-1} (Figure 9b). The systematic variations of these stretching frequencies, again, can be rationalized from the PA differences between these molecules. Since both $(C_2H_5)_2O$ and $(CH_3)_2O$ have larger proton affinities than water, they pull the excess proton farther away from the water polymers, resulting in a smaller frequency red-shift of the bonded-OH stretches of the H_3O^+ and $1°H_2O$ molecules in these two clusters.

The position of the excess proton in $H^+[(CH_3)_2O](H_2O)_n$ is a sensitive function of cluster size as illustrated in Figure 8. The proton is initially localized on dimethyl ether at $n = 1$, delocalized between $(CH_3)_2O$ and $(H_2O)_n$ at $n = 2$, and finally transferred to the water polymers at $n \geq 3$. At $n = 4$, the cluster can form either a noncyclic or a four-membered ring structure, both having the excess proton firmly attached to the water molecule. Note that, in $H^+[(CH_3)_2O](H_2O)_4$, one of the low-energy isomers has the $(CH_3)_2O$ molecule situated on the second solvation shell. This isomer (**Em4III**) can be formed via the clustering channel of **Em3II** + $H_2O \rightarrow$ **Em4III** by attaching the fourth water molecule to the $1°H_2O$ in **Em3II**. The attachment, in effect, carries the excess proton away from the ether. It is an analogous event to the proton-transfer reaction in liquid water, where an H^+ can be released from an original proton carrier via a series of hydrogen bond breaking and reforming processes.[11]

The behavior of intracluster proton transfer depends strongly on the electronic properties of the protonated bases of interest. For two bases with similar proton affinities, their proton-transfer behaviors can substantially differ owing to the difference in solvation structure. Ammonia, for example, has a proton affinity of 204.0 kcal/mol,[12] comparable to that of diethyl ether. Cheng[40] has performed molecular dynamics simulations of the solvation-induced proton-transfer effect in $NH_4^+(H_2O)_n$ and reported that the transfer can occur at $n = 4$ if all the water molecules were situated on one side of the ion core. The calculation, however, is somewhat impractical since the ammonium ion does not contain any hydrophobic groups or electron lone pairs to favor the asymmetric clustering of water molecules around NH_4^+. Recent infrared spectroscopic measurements indeed demonstrated that the hydration of NH_4^+ is fairly isotropic,[41] rendering the formation of a symmetric double-ring isomer of $NH_4^+(H_2O)_6$ available in a supersonic expansion.[24] The solvation-induced proton transfer, therefore, does not occur in the hydrated ammonia clusters.

One can extend the present study by using $(CH_3)_3N$ as a solute molecule. The hydration of this strong base is highly asymmetric, similar to that of $(CH_3)_2O$. The proton transfer in $H^+[(CH_3)_3N](H_2O)_n$, however, is expected to occur at a larger n since trimethylamine has a PA of 225 kcal/mol. One unique feature of this cluster system is that the proton transfer would eventually reverse at a certain n, since $(CH_3)_3N$ is basic in aqueous solutions with a $pK_b = 8.92$.[12] Where such a turning point is located is an interesting question to address and deserves further examination.

Conclusion

This work presents infrared spectroscopic evidence of proton transfer in protonated solute-containing water clusters in the gas phase. Systematic analysis of the spectra of $H^+(H_2O)_{n+1}$,[33] $H^+[(CH_3)_2O](H_2O)_n$, and $H^+[(C_2H_5)_2O](H_2O)_n$ reveals that the frequencies of hydrogen-bonded-OH stretches of the solvent water molecules can be used as a sensitive probe for the location of the excess proton in these clusters. We demonstrated, both theoretically and experimentally, that dimethyl ether (and also diethyl ether) can be more acidic than water in aqueous solutions. Furthermore, the proton can migrate from the protonated ether to water at a much smaller cluster size than previously anticipated from mass spectrometric studies.[26] The present studies have provided fundamental insight into the physical origin of the marked basicity change of a molecule when dissolved in solution phases. Extending the exploration to protonated water clusters containing biologically important species is an appealing direction for future work.

Acknowledgment. The authors thank the Academia Sinica and the National Science Council (Contract No. NSC 87-2113-M-001-036) of Taiwan, Republic of China, for financial support.

JA983353V

(40) Cheng, H.-P. *J. Chem. Phys.* **1996**, *105*, 6844.
(41) Chang, H.-C.; Wang, Y.-S.; Lee, Y. T.; Chang, H.-C. *Int. J. Mass Spectrom.* **1998**, *180*, 91.